

# Narrow autoresonant magnetization structures in finite length ferromagnetic nanoparticles

A. G. Shagalov<sup>1\*</sup> and L. Friedland<sup>2†</sup>

<sup>1</sup>*Institute of Metal Physics, Ekaterinburg 620990, Russian Federation and Ural Federal University, Mira 19, Ekaterinburg 620002, Russian Federation and*

<sup>2</sup>*Racah Institute of Physics, Hebrew University of Jerusalem, Jerusalem 91904, Israel*

The autoresonant approach to excitation and control of large amplitude uniformly precessing magnetization structures in finite length easy axis ferromagnetic nanoparticles is suggested and analyzed within the Landau-Lifshitz-Gilbert model. These structures are excited by using a spatially uniform, oscillating, chirped frequency magnetic field, while the localization is imposed via boundary conditions. The excitation requires the amplitude of the driving oscillations to exceed a threshold. The dissipation effect on the threshold is also discussed. The autoresonant driving effectively compensates the effect of dissipation, but lowers the maximum amplitude of the excited structures. Fully nonlinear localized autoresonant solutions are illustrated in simulations and described via an analog of a quasi-particle in an effective potential. The precession frequency of these solutions is continuously locked to that of the drive, while the spatial magnetization profile approaches the soliton limit when the length of the nanoparticle and the amplitude of the excited solution increase.

## I. INTRODUCTION

The progress in nanotechnology of magnetic materials stimulates theoretical and experimental research of new magnetic nanostructures [1]. It is well known that the fundamental model of magnetization dynamics, the Landau-Lifshitz equation, has a variety of exact solutions [2] and exhibits spatially localized objects – solitons. In the small amplitude limit, these objects were studied experimentally in thin magnetic films [3–6]. In these applications, the solitons comprise stretched configurations and long wavelength nonlinear Schrödinger (NLS) equation provides an adequate model to interpret experimental observations [2, 7]. In nanomagnetism, the NLS approximation for small amplitude solitons was also used in Refs. [8, 9]. In contrast, large amplitude solitons have small spatial widths and can be observed on nanoscales only, requiring new methods of excitation and observation. These widths can be comparable to the typical length in magnetic materials, i.e., the width of the domain walls (usually, of order of  $10\text{nm}$ ). On the other hand, nanoscale samples allow to model quasi-one-dimensional (1D) configurations [1], which are frequently used in theoretical studies of solitons [2] and guarantee their stability.

In this work, we propose the autoresonant approach to excitation of large amplitude, uniformly rotating, narrow magnetic structures in *finite length* easy axis ferromagnetic nanoparticles by using a weak, spatially uniform, chirped-frequency oscillating magnetic field. The autoresonance is a universal phenomenon used in numerous applications in many fields of physics, e.g. in particle accelerators [10, 11], atomic physics [12, 13], plasmas [14], and nonlinear waves [15]. A survey of mathematical

problems associated with autoresonance can be found in Ref. [16]. In recent years, autoresonance ideas were also implemented in magnetics. Examples are autoresonant waves in magnetic materials [17, 18], the switching of magnetization of single domain *point-like* nanoparticles [19, 20], and most recently the autoresonant excitation of large amplitude standing magnetization waves in long ferromagnetic nanowires by using rotating driving fields with short wavelength spatial modulations [21]. This recent approach required two resonant stages, where in the first stage one excites a rotating, but uniform magnetization of the wire, while later, in the second resonant stage, the system develops a spatially modified standing wave profile. In contrast, in the present work we study autoresonant formation of localized magnetization structures in finite length nanoparticles using a single resonance stage and without the need of a short wavelength modulation of the driving field. The localization in this case is imposed via boundary conditions. All these modifications require a different theory, but the simplicity of the driving scheme is expected to facilitate the realization of the idea in nanoscale magnets.

The paper is organized as follows. In Sec. II, we describe our model based on the driven Landau-Lifshitz-Gilbert (LLG) equation. A weakly nonlinear Lagrangian formulation in the dissipationless limit of this model will be used to calculate the threshold driving amplitude for autoresonant excitation of localized magnetic structures in Sec. III. Whitham’s averaged variational approach [22] will be used in the calculation. Section IV will focus on the effect of the dissipation on the threshold. A fully nonlinear, slow autoresonant dynamics of narrow chirped-driven magnetization structures will be discussed in Sec. V and, finally, Sec. VI will summarize our findings.

\* shagalov@imp.uran.ru

† lazar@mail.huji.ac.il

## II. AUTORESONANT EXCITATION MODEL

We consider a quasi-one-dimensional ferromagnetic nanoparticle of length  $L$  oriented along the  $z$ -axis. The particle has an easy-axis anisotropy along  $z$  and is located in a constant external magnetic field  $\mathbf{H} = H_0 \hat{\mathbf{e}}_z$  combined with a weak uniform rotating driving field  $\mathbf{H}_d(t) = g(\cos \varphi_d \hat{\mathbf{e}}_x + \sin \varphi_d \hat{\mathbf{e}}_y)$  having slowly chirped rotation frequency  $\omega_d(t) = -\partial \varphi_d / \partial t$ . We model this system by LLG equation (in dimensionless form):

$$\mathbf{m}_\tau = \mathbf{h} \times \mathbf{m} + \eta \mathbf{m} \times \mathbf{m}_\tau, \quad (1)$$

where  $\mathbf{m} = \mathbf{M}/M$  is the normalized magnetization,  $\eta$  is the damping parameter, and

$$\mathbf{h} = \mathbf{m}_{\xi\xi} + (m_z + h_0) \hat{\mathbf{e}}_z + \varepsilon (\cos \varphi_d \hat{\mathbf{e}}_x + \sin \varphi_d \hat{\mathbf{e}}_y). \quad (2)$$

Here and throughout the rest of the text  $(\dots)_\tau$  and  $(\dots)_\xi$  denote partial derivatives with respect to  $\tau$  and  $\xi$ . We use dimensionless time  $\tau = (\gamma K/M)t$  and coordinate  $\xi = z/\delta$ , ( $\delta = \sqrt{A/K}$ ), where  $\gamma$ ,  $A$ , and  $K$  are the gyromagnetic ratio, the exchange constant, and the anisotropy constant, respectively. In Eq. (2),  $h_0 = MH_0/K$ ,  $\varepsilon = Mg/K$ ,  $\varphi_d = -\int \Omega_d d\tau$ ,  $\Omega_d(\tau) = \omega_d M/(K\gamma)$ . We also assume that initially the magnetization  $m_z(\xi, 0) = 1$  is uniform, while at the ends  $\xi = 0$  and  $\xi = l = L/\delta$  of the particle remains fixed ( $m_z = 1$ ) at all times. An approach to realization of these boundary conditions will be discussed in Sec. V.

As in many other driven nonlinear systems [25], the autoresonant excitation of rotating localized magnetization structures requires (a) slow passage of the driving frequency  $\Omega_d(\tau)$  through a resonant frequency  $\Omega_0$ , in our case,  $\Omega_0 = 1 + k^2 + h_0$  (here  $k = \pi/l$ ), and (b) that the driving amplitude  $\varepsilon$  exceeds some threshold value  $\varepsilon_{th}$ . In particular, in the simplest case  $\Omega_d(\tau) = \Omega_0 - \alpha\tau$ , we expect the characteristic scaling  $\varepsilon_{th} \sim \alpha^{3/4}$  [25], where  $\alpha$  is the driving frequency chirp rate. When these two conditions are met, the driven magnetic perturbation will be captured into a continuing nonlinear resonance (phase-locking) with the drive, leading to large amplitude excitations of the magnetization, as the frequency chirp continues. An example of a system under consideration could be a Permalloy sample with  $A = 10^{-11} \text{ J/m}$ ,  $K = 10^5 \text{ J/m}^3$ , and  $M = 8 \times 10^5 \text{ A/m}$  [26]. In this case, the characteristic magnetic length is  $\delta \approx 10 \text{ nm}$  and the exchange length  $\delta_m = 2\sqrt{A/\mu_0 M_0^2} \approx 7 \text{ nm}$ . It is well known that the value  $\pi\delta$  represents a typical width of domain walls. The solitons in easy-axis magnets [2] can be interpreted as two interacting domain walls of opposite topological signs (a "breather" in terms of Ref. [1]) and the soliton width can be estimated as  $2\pi\delta$ . A simplest nanoparticle, where large amplitude narrow magnetic structures having near soliton spatial profiles can be observed is a segment of a ferromagnetic nanowire of length  $L > 2\pi\delta$  and cross-section  $d < 2\pi\delta_m$ . The small cross-section guarantees quasi-one-dimensionality of the system [1] in the direction of the segment, which is assumed in our model [Eqs. (1) and (2)].

## III. THE THRESHOLD PHENOMENON

We proceed by illustrating the autoresonant excitation and the threshold phenomenon in system (1) in numerical simulations. We used the numerical approach described in Ref. [21]. The simulations solved an equivalent system of two coupled NLS-type equations based on the quantum two-level analog due to R. Feynman [23]. The numerical scheme used a standard pseudospectral method [24] subject to given initial and boundary conditions,  $m_z(\xi, 0) = 1$  and  $m_z(0, \tau) = m_z(l, \tau) = 1$ . In the following illustration, we neglected dissipation and used the driving frequency  $\Omega_d(\tau) = h_0 + \Omega'_d(\tau)$ , where

$$\Omega'_d = \begin{cases} 1 + k^2 - \Delta\omega \sin(\alpha\tau/\Delta\omega), & \tau < \pi\Delta\omega/(2\alpha), \\ 1 + k^2 - \Delta\omega, & \tau > \pi\Delta\omega/(2\alpha), \end{cases} \quad (3)$$

yielding a quasi-steady-state solution in the final stage of excitation, as  $\Omega'_d(\tau)$  approached a constant. The parameters were  $\alpha = 0.005$ ,  $l = 8$ , and  $\Delta\omega = 0.9$ . Figure 1 shows  $-m_z = -\cos\theta$  and phase mismatch  $\Phi = \Phi = \varphi - \varphi_d$  ( $\theta$  and  $\varphi$  being the spherical coordinates of the magnetization vector) versus slow time  $T = \sqrt{\alpha}\tau$  just above ( $\varepsilon = 1.05\varepsilon_{th}^0$ ) and below ( $\varepsilon = 0.95\varepsilon_{th}^0$ ) the threshold  $\varepsilon_{th}^0 = 0.01$  [see Eq. (17)]. Panels a,b in the figure demonstrate the excitation of a localized large amplitude magnetic structure, which is phase-locked to the drive. In contrast, in panels c,d for  $\varepsilon < \varepsilon_{th}^0$ , phase-locking is destroyed and the excitation saturates at some small amplitude.

In analyzing the autoresonance threshold in the problem analytically, we first use the dissipationless limit of Eqs. (1) in spherical coordinates:  $m_x = \sin\theta \cos\varphi$ ,  $m_y = \sin\theta \sin\varphi$ ,  $m_z = \cos\theta$ :

$$\theta_\tau = \Phi_{\xi\xi} \sin\theta + 2\Phi_\xi \theta_\xi \cos\theta - \varepsilon \sin\Phi, \quad (4)$$

$$\Phi_\tau = -\frac{\theta_{\xi\xi}}{\sin\theta} + \Phi_\xi^2 \cos\theta + \cos\theta - \Omega'_d - \varepsilon \cot\theta \cos\Phi. \quad (5)$$

The boundary conditions are  $\theta(0) = \theta(l) = 0$ . Equations (4), (5) satisfy the variational principle with the Lagrangian density

$$\Lambda = \frac{1}{2}(\theta_\xi^2 + \Phi_\xi^2 \sin^2\theta) + \Phi_\tau \cos\theta + \Omega'_d(\tau) \cos\theta - \frac{1}{4} \cos(2\theta) - \varepsilon \sin\theta \cos\Phi, \quad (6)$$

which allows to write Eqs. (4), (5) as

$$\left( \frac{\partial \Lambda}{\partial \Phi_\tau} \right)_\tau + \left( \frac{\partial \Lambda}{\partial \Phi_\xi} \right)_\xi = \frac{\partial \Lambda}{\partial \Phi}, \quad (7)$$

$$\left( \frac{\partial \Lambda}{\partial \theta_\xi} \right)_\xi = \frac{\partial \Lambda}{\partial \theta}. \quad (8)$$

Since the autoresonance threshold is a weakly nonlinear phenomenon [20], our next goal is to discuss the slow, weakly nonlinear evolution in the problem and we use Whitham's averaged Lagrangian approach [22] for

achieving this goal. This approach is designed to describe wave systems with slow parameters. In our case the *slow* parameter is the driving frequency  $\Omega_d(\tau)$  and the slowness means that this frequency does not change significantly during one period of the driving, i.e.  $\frac{2\pi}{\Omega_d^2} \frac{d\Omega_d}{d\tau} \ll 1$ . We seek *rapidly* rotating solution, such that  $\varphi_t \approx \Omega_d(\tau)$ , but assume that the phase mismatch  $\Phi(\tau) = \varphi - \varphi_d$  is slow (i.e., experiences only a small change during one period of the drive). Since in the linear approximation and constant  $\Omega_d$ , Eqs. (4), (5) yield a phase-locked driven solution

$$\theta = a \sin(k\xi), \Phi = \pi$$

where  $a = \varepsilon/(\Omega'_d - 1 - k^2)$ , in the *slowly varying*  $\Omega_d$  problem, we use the following *small* amplitude ansatz

$$\theta = a(\tau) \sin \Theta, \Phi = f(\tau) + b(\tau) \sin \Theta. \quad (9)$$

Here  $\Theta = k\xi$  and it is assumed that the weak nonlinearity, small driving, and slow variation of the driving frequency introduce slow time dependence in  $a$ ,  $b$  and  $f$ . Note that this ansatz is just a truncated Fourier expansion conserving the boundary conditions and that for  $k = \pi/l$ , the length  $l$  of the nanoparticle is one half of the periodicity length  $l_0 = 2\pi/k$  in (9). At this stage, for simplifying the derivation, we will set  $b = 0$ , but later

show that to lowest order, inclusion of nonzero  $b$  does not introduce a significant change in the weakly nonlinear theory. The substitution of (9) into (6), the expansion to fourth order in  $a$ , and averaging over  $\Theta \in [0, \pi]$  yields the averaged Lagrangian density

$$\bar{\Lambda} = \frac{a^2}{4}(1 + k^2 - \Omega'_d - \beta) + \frac{a^4}{64}(-4 + \Omega'_d + \beta) - \frac{2}{\pi}a\varepsilon \cos f, \quad (10)$$

where  $\beta = f_\tau$  and we omitted terms independent of  $f$  and  $a$ , as not contributing the dynamics. Note that Eqs. (9) involve only slow time dependencies and, thus, there is no need for averaging the Lagrangian over the fast oscillations. Next, we use  $\bar{\Lambda}$  and take variation with respect to  $f$ , leaving lowest significant order terms only to get

$$\frac{da}{d\tau} = -\frac{4\varepsilon}{\pi} \sin f. \quad (11)$$

Here and in the next section the problem depends on  $\tau$  only, so the time derivatives are now defined as  $d(\dots)/d\tau$ . Similarly, the variation with respect to  $a$  yields the second evolution equation

$$\beta = \frac{df}{d\tau} = 1 + k^2 - \Omega'_d - \frac{4 - \Omega'_d}{8}a^2 - \frac{4\varepsilon}{\pi a} \cos f. \quad (12)$$

Note that the frequency of rotation of the magnetization vector in the linearized undriven problem is  $h_0 + 1 + k^2$  and assume passage through the linear resonance, i.e.  $\Omega'_d = \Omega_d - h_0 = 1 + k^2 - \alpha\tau$ , where  $\alpha\tau$  is viewed as a small deviation of the driving frequency from the resonance. Then Eqs. (11) and (12) guarantee the assumed slowness of variation of  $a$  and  $f$  if the nonlinearity and driving amplitude  $\varepsilon$  and chirp rate  $\alpha$  are sufficiently small. Next, we introduce rescaled amplitude  $A = [(3 - k^2)/8]^{1/2} \alpha^{-1/4} a$ . This allows to rewrite Eqs. (11) and (12) as

$$\frac{dA}{dT} = -\mu \sin f, \quad (13)$$

$$\frac{df}{dT} = T - A^2 - \frac{\mu}{A} \cos f, \quad (14)$$

where  $T = \alpha^{1/2}\tau$  is the slow time (used in Figs. 1 and 2), and

$$\mu = \frac{[2(3 - k^2)]^{1/2} \varepsilon}{\pi \alpha^{3/4}}. \quad (15)$$

By introducing a complex dependent variable  $\Psi = Ae^{if}$ , Eqs. (13) and (14) can be combined into a single equation characteristic of many autoresonance problems [25]:

$$i \frac{d\Psi}{dT} + (T - |\Psi|^2)\Psi = \mu. \quad (16)$$

If starting in zero equilibrium  $\Psi = 0$  at  $T < 0$  (above the linear resonance), this equation guarantees phase locking at  $f \approx \pi$  after passage through the resonance (i.e., for  $T = 0$ ), where  $A$  increases as  $\sim \sqrt{T}$ , provided the single

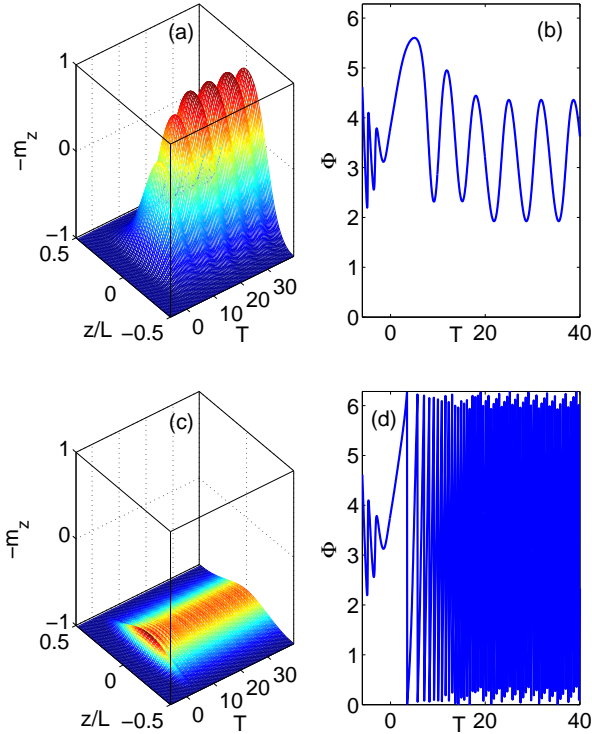


FIG. 1: The magnetization component  $-m_z$  and phase mismatch  $\Phi$  versus slow time  $T = \alpha^{1/2}t$ . (a) and (b) just above the threshold,  $\varepsilon = 1.05\varepsilon_{th}^0$ . (c) and (d) just below the threshold,  $\varepsilon = 0.95\varepsilon_{th}^0$ .

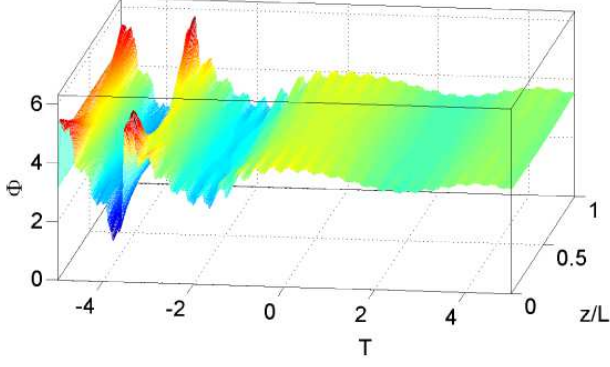


FIG. 2: The disappearance of the spatial modulation of  $\Phi$  after entering the autoresonance regime

parameter  $\mu$  in the problem exceeds the value of 0.41 [20]. This yields the threshold driving amplitude

$$\varepsilon_{th}^0 = \frac{0.41\pi\alpha^{3/4}}{[2(3-k^2)]^{1/2}}. \quad (17)$$

The results in Fig. 1 illustrate that this threshold is in a good agreement with numerical simulations.

Next, we include the spatial variation in  $\Phi = f(\tau) + b(\tau) \sin \Theta$  in calculating the averaged Lagrangian density. This results in the addition of a new,  $b$ -dependent part

$$\bar{\Lambda}_b(a, f, b, b_\tau) = \frac{2}{3\pi}a^2b_\tau + \frac{\varepsilon}{2}ab \sin f + \frac{k^2}{16}a^2b^2 \quad (18)$$

to already discussed Lagrangian density (10). By taking the variation with respect to  $b$ , we now get a new evolution equation

$$\frac{da}{d\tau} = -\frac{3\pi}{8}\varepsilon \sin f - \frac{3\pi k^2}{32}ab. \quad (19)$$

Then, on using Eq. (11), one obtains

$$ab = \frac{32}{3\pi k^2} \left( \frac{4}{\pi} - \frac{3\pi}{8} \right) \varepsilon \sin f = \frac{0.32}{k^2} \varepsilon \sin f. \quad (20)$$

This result shows that  $b$  becomes negligibly small as  $a$  increases and significantly exceeds  $\varepsilon$  in the autoresonant stage, validating the derivation of the threshold driving amplitude presented above. This effect is illustrated in Fig. 2, showing the spatial form of  $\Phi$  versus slow time  $T$  for parameters  $\varepsilon = 0.02$ ,  $\alpha = 0.005$ ,  $L = 8$ , and  $\Delta\omega = 1$ . One can see how the spatial modulation of  $\Phi$  nearly disappears after the passage through the linear resonance at  $T = 0$  and entering the autoresonant stage of evolution.

#### IV. EFFECT OF DISSIPATION

For including a weak dissipation in the calculation of the threshold, we return to the original system of evolution equations with Gilbert damping

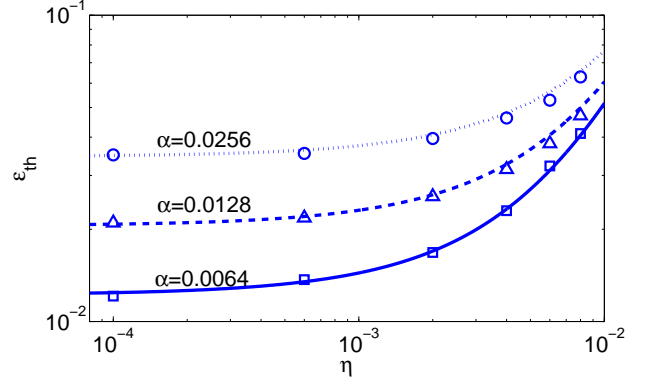


FIG. 3: The effect of the dissipation on the threshold for capture into autoresonance. The lines are given by Eq. (27) and the markers represent numerical simulations.

$$\left( \frac{\partial \Lambda}{\partial \Phi_\tau} \right)_\tau + \left( \frac{\partial \Lambda}{\partial \Phi_\xi} \right)_\xi - \frac{\partial \Lambda}{\partial \Phi} = -\eta \varphi_\tau \sin^2 \theta, \quad (21)$$

$$\left( \frac{\partial \Lambda}{\partial \theta_\xi} \right)_\xi - \frac{\partial \Lambda}{\partial \theta} = \eta \theta_\tau. \quad (22)$$

Here the left hand sides are the Lagrange's components of the dissipationless case described by the Lagrangian density (6) and, as before,  $\varphi = \Phi + \varphi_d$  is the azimuthal angle of the magnetization vector. Within the ansatz  $\Phi = f(\tau)$  and  $\theta = a(t) \sin \Theta$  discussed above, Eq. (21) yields

$$\theta_\tau \sin \theta + \varepsilon \sin \theta \sin \Phi = \eta(\Phi_\tau - \Omega_d) \sin^2 \theta, \quad (23)$$

where  $\Omega_d = d\varphi_d/d\tau = \Omega_0 - \alpha\tau$  is the driving frequency. On averaging the last equation with respect to  $\Theta \in [0, \pi]$ , one obtains

$$\frac{da}{d\tau} = -\frac{4\varepsilon}{\pi} \sin f - \eta a \Omega_d, \quad (24)$$

where, assuming a continuing phase-locking ( $\Phi$  remains nearly constant), we neglected  $\Phi_\tau$  in the right hand side. The last equation replaces Eq. (11) of the dissipationless case. Furthermore, this equation shows that the right hand side of Eq. (22) involves a product of two small objects and can be neglected in the following. Thus, the additional evolution equation [originating from (22)]

$$\frac{df}{d\tau} = \alpha\tau - \frac{3-k^2}{8}a^2 - \frac{4\varepsilon}{\pi a} \cos f, \quad (25)$$

is the same as Eq. (12) for the dissipationless case.

Using the rescaling of the dependent and independent variables of the dissipationless case, Eqs. (24) and (25) can be combined into a single complex equation [compare to Eq. (16)]

$$i \frac{d\Psi}{dT} + (T - |\Psi|^2)\Psi + i \frac{\gamma}{2}\Psi = \mu, \quad (26)$$

where  $\gamma = 2\eta\Omega_d\alpha^{-1/2}$ . The capture into autoresonance in this problem was studied in Ref. [27], yielding the following threshold driving amplitude for  $\gamma < 1$ .

$$\varepsilon_{th} \approx \varepsilon_{th}^0 (1 + 1.06\gamma + 0.67\gamma^2). \quad (27)$$

We compare this result with the numerical simulations of the original LLG equation in Fig. 3, showing  $\varepsilon_{th}$  versus  $\eta$  for three values of the chirp rate  $\alpha = 0.0064, 0.0128$ , and  $0.0256$ . We used parameters  $l = 8$ ,  $\Delta\omega = 0.9$ ,  $h_0 = 5$  and frequency variation of the form (3). The simulation was limited to values of  $\gamma < 1$  and used the initial and final simulation times  $T_0 = -10$  and  $T_1 = 30$ , respectively, reaching the quasi-steady-state at the final time. Arriving in simulations at this quasi-steady-state without dephasing served as the criterion for finding  $\varepsilon_{th}$ .

## V. NONLINEAR QUASI-STEADY-STATE

In our numerical simulations (e.g., Fig.1) we observe that in the autoresonant stage of evolution, both  $\Phi$  and  $\theta$  perform slow oscillations around some smooth time varying averages. We will refer to the smooth evolution as the quasi-steady-state (it still slowly varies in time). Similar slow oscillations around the smooth average were observed and studied in many autoresonant problems [25] and reflect the stability of the quasi-steady-state if perturbed. The problem of stability of fully nonlinear autoresonant evolution is important, but very complex in our case and will remain outside the scope of the present work and, thus, we focus on describing the quasi-steady-state only. We proceed from Eqs. (4) and (5) and assume a perfect continuing phase-locking,  $\Phi = \pi$  (uniform precession of the magnetization vector,  $\varphi_t = \Omega'_d(\tau)$ ), and neglect  $\theta_\tau$  despite the time variation of the driving frequency. This leaves us with a single equation

$$\theta_{\xi\xi} = -V_\theta, \quad (28)$$

where we have also neglected the driving term and defined the effective potential

$$V = -\Omega'_d(\tau) \cos \theta + \frac{1}{4} \cos(2\theta) - \left[ \frac{1}{4} - \Omega'_d(\tau) \right]. \quad (29)$$

We have added a shift in  $V$  so that  $V = 0$  at  $\theta = 0$  at all times, which is convenient for classifying different types of solutions (see below). Equation (28) can be viewed as defining the motion of a quasiparticle having coordinate  $\theta$  in the effective potential  $V$ ,  $\xi$  playing the role of time and  $\Omega'_d(\tau)$  being a parameter. The solution of (28) subject to boundary conditions  $\theta = 0$  ( $m_z = 1$ ) at  $\xi = 0, l$ , corresponds to a *single* round trip of the quasiparticle in the effective potential starting from  $\theta = 0$  at  $\xi = 0$  and returning to the same point  $\theta = 0$  at  $\xi = l$ .

The form of the quasi-potential allows to qualitatively describe the motion of the quasiparticle in the problem. Note that for  $\Omega'_d < 1$  the quasipotential has a zero maximum at  $\theta = 0$ , a minimum  $V_{\min} = -(\Omega_d'^2/2 + 1/4)$

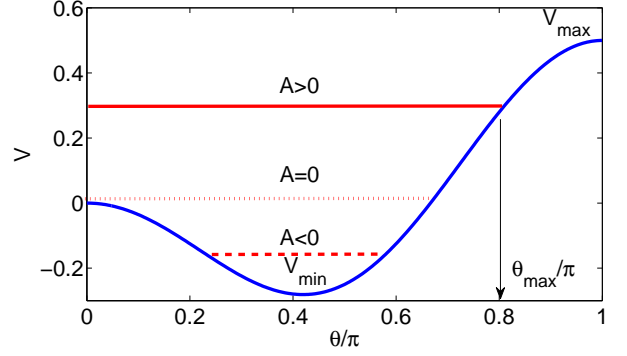


FIG. 4: The effective potential. Two classes of oscillations correspond to different values of the quasi-energy:  $A > 0$  (solid horizontal line) is the case of the zero boundary conditions used in this work,  $A < 0$  (dashed horizontal line) is the standing magnetization wave of Ref. [21]. The limit  $A \rightarrow 0$  (dotted horizontal line) corresponds to the soliton solution of infinite extent ( $\lambda \rightarrow \infty$ ).

at  $\cos \theta = \Omega'_d$ , and another maximum  $V_{\max} = 2\Omega'_d$  at  $\theta = \pi$ , as illustrated in Fig. 4 for  $\Omega'_d = 0.25$ . Therefore, the quasiparticle passes  $\theta = 0$  (i.e. one satisfies the boundary conditions  $\theta = 0$  at  $\xi = 0$  and  $l$ ) provided (a)  $V_{\max} > 0$  (i.e. the allowed range of  $\Omega'_d$  is  $0 < \Omega'_d < 1$ ) and (b) the quasi-energy  $A(\tau) = \frac{1}{2}\theta_\xi^2 + V$  is in the interval  $[0, V_{\max}]$  (see the solid red horizontal line in Fig. 4). The solutions for  $\theta(\xi)$  in this case have a single maximum and a finite extent in  $\xi$ . In addition to this type of solutions, there also exists a motion of the quasiparticle, such that  $V_{\min} < A < 0$  (see the horizontal red dashed line in Fig. 4), but this motion does not reach  $\theta = 0$  and, thus, can not satisfy our boundary conditions. Autoresonant magnetic excitations of this different type were discussed in Ref. [21] and comprise spatial oscillations of  $\theta$  having a finite periodicity length. Interestingly, the two types of solutions coalesce in the limit  $A \rightarrow 0$  (the dotted red line in Fig. 4) and  $\theta(\xi)$  assumes a form of a single peak defined on the infinite  $\xi$  domain, i.e a soliton (see Ref [2]). The physical width of  $\theta$  in this limit can be estimated as

$$\Delta\xi \approx 2\pi/\kappa_m, \quad (30)$$

where  $\kappa_m = (1 - \Omega_d'^2)^{1/2}$  is the frequency of linear oscillations around the minimum of  $V$ . For example, if  $0 < \Omega'_d < 0.5$ , one has  $2\pi < \Delta\xi < 7.25$ . In our case of a finite length of the nanoparticle,  $\theta(\xi)$  can only approximately approach the form of the soliton, but, nevertheless, Eq. (30) can still be used as an estimate of the width of the excited solution.

Note that Eq. (28) can be solved in quadratures for finding  $\theta(\xi, \tau)$  at a given time. However, this solution also requires the knowledge of the quasi-energy  $A(\tau) = \frac{1}{2}\theta_\xi^2 + V$ . Finding this energy, seems to require including the drive and solving the full driven PDE. Nevertheless, if the system evolves in autoresonance, one can

calculate  $A(\tau)$  by using simplified arguments. Indeed, in the autoresonance, the azimuthal frequency of magnetization follows that of the drive, while the extent  $\lambda$  of the spatial profile of  $\theta$  remains constant  $\lambda = l$ . The preservation of  $\lambda(\tau)$  at value  $l$ , despite the variation of  $\Omega'_d$  in time allows calculation of the quasi-energy at all times using the definition

$$\lambda = 2 \int_0^{\theta_{\max}} \frac{d\theta}{\sqrt{2[A(\tau) - V(\theta, \Omega'_d)]}}. \quad (31)$$

As an example, we have solved this problem numerically (for details of this calculations see Appendix) and found  $A$  for different values of  $\Omega'_d = 1 + k^2 - D$  in the case of  $l = 8$  ( $k = 0.393$ ) and  $0.7 \leq D \leq 1.05$  (recall that  $D$  represents the driving frequency deviation in all our numerical simulations). Note that  $\lambda \rightarrow \infty$  at the limiting values  $A = 0$  and  $A = V_{\max}$  and, therefore,  $\lambda$  has a minimum at some  $A$  between 0 and  $V_{\max}$ . Therefore, for having the solution of equation  $\lambda = l$ ,  $l$  must be above this minimum. We have found that such solutions in our example exists for  $D < 1.05$ . The knowledge of  $A$  allows to calculate the spatial profile  $\theta(\xi)$

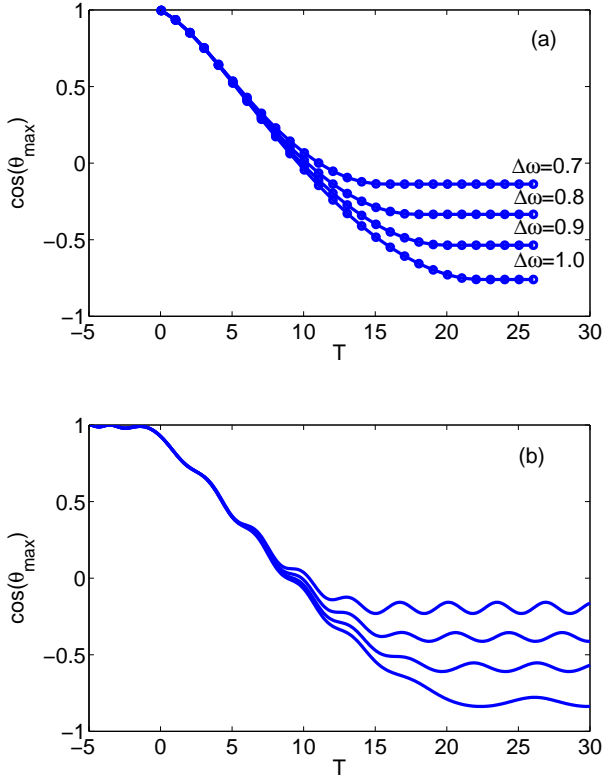


FIG. 5: The axial magnetization component  $m_z = \cos(\theta_{\max})$  at the maximum  $\theta_{\max}$  of the autoresonant excitation versus slow time  $T$ . (a) the quasi-steady-state theory, (b) numerical LLG simulations.

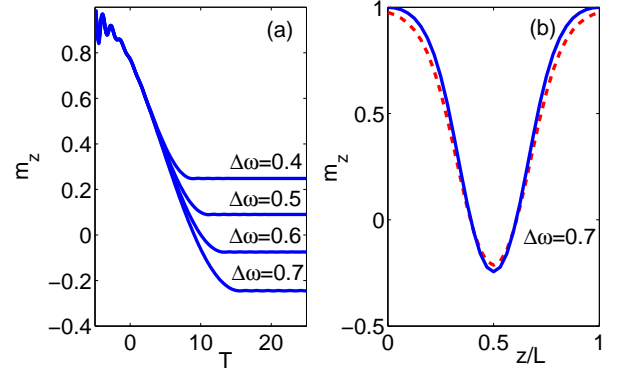


FIG. 6: The autoresonant excitation in the presence of dissipation  $\eta = 0.01$  (LLG simulations). (a) The axial magnetization component  $m_z = \cos(\theta_{\max})$  at the maximum  $\theta_{\max}$  of the autoresonant excitation versus slow time  $T$ , (b) The comparison of the excited waveform (solid line) with the exact dissipationless soliton solution [2] (dashed line).

by solving Eq. (28) in quadratures, but, for simplicity, we have limited the calculation to just finding the maximum of the autoresonant excitation  $\theta_{\max} = \theta(l/2)$  by solving  $V(\theta_{\max}) = A$  at each time. We summarize this quasi-steady-state evolution in Fig. 5a, showing  $m_z(l/2) = \cos \theta_{\max}$  (circles) versus slow time  $T$  for four values of  $\Delta\omega = 0.7, 0.8, 0.9$ , and  $1.0$ . The results are in a good agreement with the full numerical LLG simulations shown in Fig. 5b for the same  $\Delta\omega$ , confirming the quasi-steady-state theory. Note that the quasi-steady-state calculations involve solution of algebraic equations only, which is significantly simpler than the full numerical simulations.

It is interesting to compare the amplitudes of the solutions in Fig. 5a to those of the exact solitons for easy-axis magnets [2]:

$$\tan^2(\theta_{\max}/2) = \Omega'_d/(\Omega'_d - \Delta\omega) - 1. \quad (32)$$

This equation yields  $\cos(\theta_{\max}) = -0.20, -0.38, -0.56, -0.73$  for  $\Delta\omega = 0.7, 0.8, 0.9, 1.0$ , respectively, in a very good agreement with the values in Fig. 5a at the final time. It is also interesting to discuss the effect of dissipation. Figure 6a shows the results of the LLG simulations similar to those in Fig. 6b, but for  $\eta = 0.01$  and  $\Delta\omega = 0.4, 0.5, 0.6, 0.7$ . The final amplitudes  $m_z(l/2) = \cos \theta_{\max}$  of the solutions in this cases were  $0.31, 0.13, -0.04$  and  $-0.21$ . In addition, Fig. 6b shows the solution  $m_z(z/L)$  found in numerical LLG simulations (solid blue line) at  $\Delta\omega = 0.7$  and compares it to the form of the exact soliton solution (red dashed line) [2]. The good agreement in the figure shows that the boundary conditions imposed sufficiently far from the localized magnetization structure only slightly deform its shape preserving the proximity to the soliton solution, i.e., the autoresonant drive efficiently compensates for dissipation.



The amplitude of the autoresonant steady-state solutions depends on the final driving frequency shift  $\Delta\omega$ . We have found numerically that there exists some critical value  $\Delta\omega_{cr}$  such that stable phase-locked solutions can be excited for  $\Delta\omega < \Delta\omega_{cr}$  only. One finds that  $\Delta\omega_{cr}$  depends mainly on length  $l$  and weakly on  $\varepsilon$  and  $\alpha$  if  $\varepsilon > \varepsilon_{th}$ , see Fig. 7. In the dissipationless case,  $\Delta\omega_{cr}$  is close to unity for  $l > 7$  and rapidly decreases for  $l < 7$ . Note that  $l \approx 7$  is near the typical size  $\Delta\xi$  of the solitons [see Eq. (30)], while the maximum value of  $\Delta\omega_{cr} \approx 1.05$  is in agreement with  $D = 1.05$  case in Fig. 9 in the Appendix. In the dissipative case, the autoresonant driving compensates the effect of damping, providing stability of the driven phase-locked soliton. In this case,  $\Delta\omega_{cr}$  has the maximum value of 0.75 at  $l \approx 7$ , yielding the largest amplitude of the autoresonant excitation for this damping parameter. We have also found that with dissipation,  $\Delta\omega_{cr}$  rapidly decreases for  $l < 7$  and that stable solitons do not exist for  $l < 3$  with and without dissipation.

We conclude this Section by discussing the realization of the assumed boundary conditions, i.e., that the spins of the nanoparticle are 'pinned' at the boundaries ( $m_z = 1$ ). It turns out that this condition can be realized for free spins as well. Indeed, we can exploit the fact that the proposed excitation approach involves a resonant driving mechanism. Therefore, if one destroys the resonance at the ends of the nanoparticle, the magnetization of the ends will not be affected by the resonant drive and, thus, remain in the direction of the guiding magnetic field  $\mathbf{H}$  as set initially. For example, if the anisotropy of the end sections of the particle is larger than of its middle part, the ends will remain steady when the driving field is tuned to resonate with the middle section. We illustrate this approach in numerical LLG simulations in Figs. 8a and 8c showing two narrow structures of different height excited in a nanoparticle of length  $l = 100$  with the two end sections of length  $l/3$  each having (normalized) anisotropy constant of 1.25, while the anisotropy constant of the middle  $l/3$  section is 1.0, as before. In addition, Figs. 8b

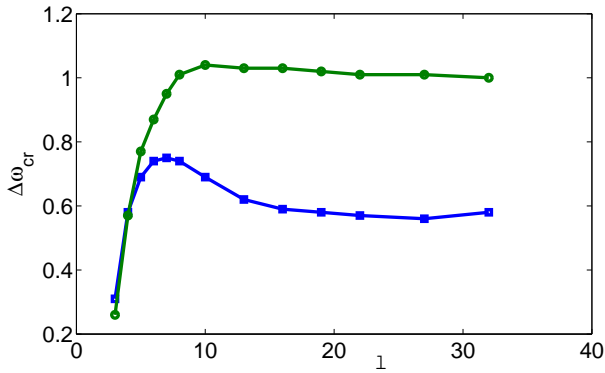


FIG. 7: The dependence of the critical driving frequency shift  $\Delta\omega_{cr}$  on  $l$ :  $\eta = 0$  (upper line) and  $\eta = 0.01$  (lower line) for  $\varepsilon = 2\varepsilon_{th}$  and  $\alpha = 0.005$ .

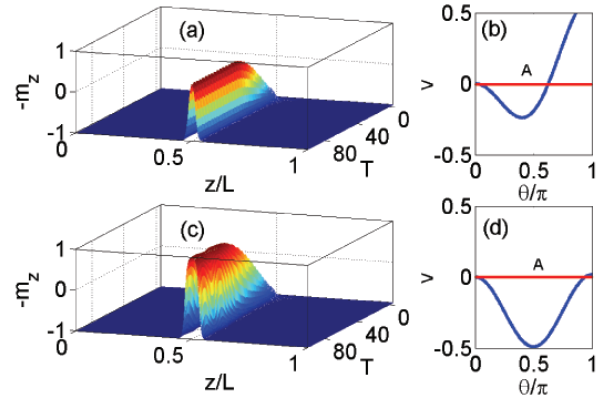


FIG. 8: The excitation of narrow magnetization structures using increased anisotropy of the end sections of the particle to preserve  $m_z = 1$  boundary conditions. Panels (a) and (c) show the  $-m_z$  for  $\Delta\omega = 0.7$  and 1.0 respectively, while panels (b) and (d) present the corresponding effective potentials  $V$  and the quasi-energies  $A$  (red horizontal lines) at final time  $T = 100$ .

and 8d show the effective potential for both excitations and the corresponding quasi-energies,  $A \approx 0$ , as expected for solitary waves. In these simulations, we set  $m_z = 1$  at  $\xi = 0, l$  initially, but did not impose this condition at later times. The figure shows two solutions of different amplitude excited along the particle for  $\Delta\omega = 0.7$  and 1.0. The rest of the parameters were  $\alpha = 0.005$ ,  $h_0 = 5$ ,  $\eta = 0.005$ ,  $\varepsilon = 1.2\varepsilon_{th}$ . As expected, the boundary condition of  $m_z = 1$  at the ends of the particle is preserved (the ends are off resonance) and the excited autoresonant solutions have a width  $\Delta\xi \approx 7$  [see Eq. (30)] much smaller than the length of the particle.

## VI. CONCLUSIONS

In conclusion, we have suggested and analyzed the autoresonant approach to excitation of LLG localized solutions in easy axis ferromagnetic nanoparticles. The approach involved driving the system under fixed boundary conditions by a spatially uniform, but oscillating magnetic field having chirped frequency, which passes through the linear resonance with initially uniform magnetization. When the driving amplitude exceeded a threshold  $\varepsilon_{th}$ , we have observed formation of large amplitude rotating magnetization structures (see Fig. 1). We have used a weakly nonlinear Lagrangian formulation in the dissipationless limit of the model for calculating the threshold [Eq. (17)] and discussed the effect of dissipation on the threshold [Eq. (27)]. All these predictions were in a good agreement with simulations. We have also analyzed fully nonlinear autoresonant quasi-steady-state localized solutions using a simple analog of a quasi-particle in an effective potential (see developments in

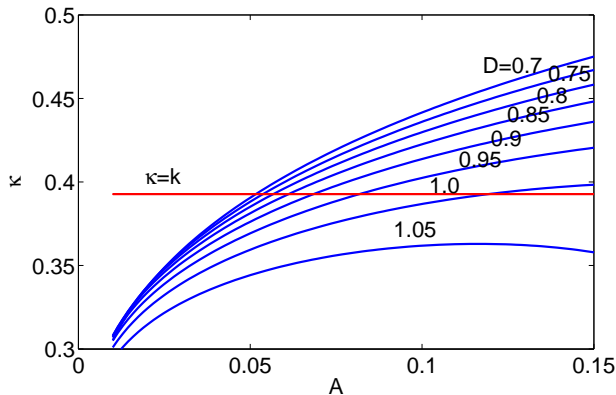


FIG. 9: The parameter  $\kappa = \pi/\lambda$  versus the quasi-energy  $A$  for different driving frequency shifts  $D$  and  $l = 8$ . Condition  $\kappa = k$  can be satisfied for  $D < 1.05$  only.

Sec. V). In these calculations, the decreasing driving frequency gradually approached some fixed target value at distance  $\Delta\omega$  from the linear resonance, which also defined the target amplitude of the excited solution. We found numerically that there exists a critical  $\Delta\omega_{cr}$ , such that the excited structures remained stable if  $\Delta\omega < \Delta\omega_{cr}$ . This critical  $\Delta\omega_{cr}$  depended mainly on the dimensionless length  $l$  and damping parameter  $\eta$  and decreased rapidly for  $l < 7$  (the approximate width of the solution). In the dissipationless case,  $\Delta\omega_{cr} \approx 1.05$ , yielding almost complete inversion of magnetization at the solution maximum. We have found that the autoresonant drive effectively compensates the effect of dissipation on the excited solutions, but the dissipation lowers their amplitude. Finally, we have suggested and illustrated an approach to realization of the assumed fixed boundary conditions by increasing the anisotropy of the end sections of the particle. A further development of the Whitham's-type variational theory in order to explain the stability (seen in simulations) of the chirped-driven large amplitude local-

ized solutions is important. Finally, it is known that the dissipationless LLG equation in 1D is integrable and has a large variety of solutions [2]. The autoresonant excitation and control of some of these solutions comprises another important goal for future research.

## VII. ACKNOWLEDGEMENT

This work was supported by the Israel Science Foundation Grant No. 30/14 and the Russian state program AAAA-A18-118020190095-4.

## VIII. APPENDIX

In calculating the quasi-energy  $A$  of the slow evolution of the autoresonant quasi-steady-state, instead of solving Eq. (31) defining  $\lambda$ , we proceed by introducing the action

$$I(A) = \frac{2}{\pi} \int_0^\pi \text{Re}[\sqrt{2(A - V)}] d\theta. \quad (33)$$

Then, since

$$\kappa = \frac{\pi}{\lambda} = \left( \frac{dI}{dA} \right)^{-1}, \quad (34)$$

we calculate the action for different values of  $\Omega'_d = 1 + k^2 - D$  and take its derivative  $(dI/dA)^{-1}$  numerically to find  $\kappa(A)$ . The results are shown in Fig. 9 in the case of  $l = 8$  ( $k = 0.393$ ) and  $0.7 \leq D \leq 1.05$ . Such calculations and using  $\Omega'_d$  of form (3) allow to find the quasi-energy  $A$  such that  $\kappa = k$  ( $\lambda = l$ ) at different times. Note that  $\kappa = 0$  at the limiting values of  $A = 0$  and  $V_{\max}$  and, therefore,  $\kappa$  has a maximum at some  $A$  between 0 and  $V_{\max}$ , as can be seen in Fig. 5 for  $D = 1.05$ . Thus, for having the solution with  $\kappa = k$  in the driven problem ( $k = 0.393$  in our example),  $k$  must be below this maximum as for  $D \leq 1.0$  in Fig. 5, while no such solution exists for  $D = 1.05$ .

- 
- [1] H.B. Braun, Adv. Phys. **61**, 1 (2012).
  - [2] A.M. Kosevich, B.A. Ivanov, A.S. Kovalev, Phys. Rep. **194**, 117 (1990).
  - [3] M.M. Scott, M.P. Kostylev, B.A. Kalinikos, C.E. Patton, Phys. Rev. B **71**, 174440 (2005).
  - [4] M. Wu, M. A. Kraemer, M.M. Scott, C.E. Patton, B.A. Kalinikos, Phys. Rev. B **70**, 054402 (2004).
  - [5] M. Wu, P. Krivosik, B.A. Kalinikos, C.E. Patton, Phys. Rev. Lett. **96**, 227202 (2006).
  - [6] M. Chen, M.A. Tsankov, J.M. Nash, C.E. Patton, Phys. Rev. Lett. **70**, 1707 (1993).
  - [7] A.K. Zvezdin, A.F. Popkov, Sov. Phys. JETP **57**, 350 (1983).
  - [8] P.B. He, W.M. Liu, Phys. Rev. B **72**, 064410 (2005).
  - [9] Zai-Dong Li, Qiu-Yan Li, Lu Li, W.M. Liu, Phys. Rev. E **76**, 026605 (2007).
  - [10] E. M. McMillan, Phys. Rev. **68**, 143 (1945).
  - [11] V. I. Veksler, J. Phys. USSR **9**, 153 (1945).
  - [12] B. Meerson and L. Friedland, Phys. Rev. A **41**, 5233 (1990).
  - [13] H. Maeda, J. Nunakaew, and T. F. Gallagher, Phys. Rev. A **75**, 053417 (2007).
  - [14] J. Fajans, E. Gilson, and L. Friedland, Phys. Plasmas **6**, 4497 (1999).
  - [15] M.A. Borich, A. G. Shagalov, L. Friedland, Phys. Rev. E **91**, 012913 (2015).
  - [16] L.A. Kalyakin. Russ.Math.Surv. **63**, 791 (2008).



- [17] M.A. Shamsutdinov, L.A. Kalyakin, A.L. Sukhonosov, A.T. Kharisov, *The Physics of Metals and Metallography*. **110**, 430 (2010).
- [18] M.A. Shamsutdinov, L.A. Kalyakin, A.T. Kharisov, *Technical Physics* **55**, 860 (2010).
- [19] G. Klughertz, P-A. Hervieux, and G. Manfredi, *J. Phys. D: Appl. Phys.* **47**, 345004 (2014).
- [20] G. Klughertz, L. Friedland, P-A. Hervieux, and G. Manfredi, *Phys. Rev. B* **91**, 104433 (2015).
- [21] L. Friedland, A.G. Shagalov, *Phys. Rev. B* **99**, 014411 (2019).
- [22] G. B. Whitham, *Linear and Nonlinear Waves* (Wiley, New York, 1974).
- [23] R. Feynman, F. L. Vernon, and R. W. Hellwarth, *J. Appl. Phys.* **28**, 49 (1957).
- [24] C. Canuto, M. Y. Hussaini, A. Quarteroni, and T. A. Zang, *Spectral Methods in Fluid Dynamics* (Springer-Verlag, New York, 1988).
- [25] L. Friedland, *Scholarpedia* **4**, 5473 (2009).
- [26] W. Wang, Z. Zhang, R. A. Pepper, C. Mu, Y. Zhou, H. Fangohr, *J. Phys.: Condens. Matter* **30**, 015801 (2018).
- [27] O. Naaman, J. Aumentado, L. Friedland, J.S. Wurtele, I. Siddiqi, *Phys. Rev. Lett.* **101**, 117005 (2008).